１．「Si基板上GaAs系レーザ特性及び信頼性改善に関する研究」

Introduction

1.1 Historical Background of GaAs on Si

After the invention of bipolar transistor (1948)[1], research on semiconductor devices drawn much attention. In the earlies of 1950, Ge was the major semiconducting material used for device fabrication. However, Ge was proved unsuitable for many application due to the resultant high leakage currents of Ge based transistors even at elevated temperature. Also the native water soluble GeO_2 lead to the difficulty in the realization of high quality devices. As an alternate to Ge, Si emerged and the (i) easily refinable, (ii) easy growth behavior of high quality large size Si single crystal, (iii) possible nano-processing, (iv) exhibition of stable device characteristics, (v) structural protection of Si devices by its native SiO_2 growth and (vi) success of fabricating two dimensionally integrated devices structure are the advantage of Si over Ge. Above such properties of Si lead to realize very high quality devices in submicron size with integration to very large scale (VLSI)[2]. Apart from the superior material properties, there is also economic consideration. Si is available on the earth in the form of silica and silicates comprises 25% of the earth's crust and only Si is the second to oxygen in abundance, which leads to the low production cost for integrated circuits. Even though Si has potential dominance in electronic industry, low carrier mobility, indirect energy band-structure and the low probability of optical transition of Si, prevent to realize high speed devices, optical devices like LEDs, laser diodes, photodetectors for optical communication and microwave applications, etc..

In 1952, H. Welker[3] reported about the "man-made crystal" in which he reported about the combination of group IIIb (B, Al, Ga, In) and group Vb (N, P, As, Sb) elements of the periodic table to form "compound". The carriers in

compound semiconductors have in general smaller effective mass than those in Si and Ge, leading to higher mobilities. An additional important property of some compound semiconductors is that the band-gap energy can be varied without changing the lattice constant.

In the beginning of 1962, Pankove demonstrated the first GaAs *p-n* junction infra-red radiation source as a first GaAs based device[4,5]. Later, Nasledov and coworkers reported that the line-width of the radiation emitted from GaAs diodes narrowed slightly at high current densities and suggested that this might be a sign of stimulated emission[6]. In the same year 1962, Hall and his coworkers succeeded in making the first semiconductor laser[7].

As a state of art, high performance devices using AlGaAs/GaAs heterojunctions such as lasers[8], solar cells[9], FETs[10] etc., have been fabricated on GaAs substrates. If these devices were grown on Si substrate with high performance, the new devices such as opto-electronic ICs that contain GaAs optical and Si electronic devices, GaAs IC on large area Si substrate and many other devices combining GaAs and Si would become realistic in order to couple the low cost and high performance materials together.

1.2. Epitaxial Growth Processes

There are four main techniques by which GaAs and AlGaAs epitaxial films are grown : Chloride transport vapor phase epitaxy (VPE)[11], liquid phase epitaxy (LPE)[12], molecular beam epitaxy (MBE)[13] and metalorganic chemical vapor deposition (MOCVD)[14].

In the chloride transport VPE growth system, silicon contamination is serious and which, creates unfavorable thermodynamics in the growth of compounds, destroy the quality of the epilayer for device fabrication. The LPE technique, though it has been successfully used in compound semiconductors, is not suitable for mass production due to the limitation in the growth area and also

the abruptness of the GaAs interface grown by LPE is unsatisfactory for high-speed device fabrication due to the cross contamination[15].

MBE is considered to be the most promising future growth technique because it allows for precise thickness, dopant control and pattern drawing[16]. Growth is performed under an ultra-high vacuum chamber with a low growth rate (0.1 to 10 μm/h) and it permits the accurate control of the impinging atoms or molecules and thus thickness of the film[17].

The MOCVD technique has demonstrated as efficient epitaxial growth method for the widest variety of III-V materials and device structures with the following advantages[18,19] : (1) the formation of the desired compound occurs via the pyrolysis of the metalorganics and hydrides, and subsequent recombination of the atomic or molecular species occur at or near the substrate surface, (2) The composition and impurity concentration can be controlled precisely by fixing the flow rates of the various reactants with electronic mass flow controllers, (3) complex multilayer epitaxial structures are readily formed by exchanging one gas composition to another gas using automatic gas mixing system, (4) this technique is suitable for mass production based on its similarity to silicon CVD process. The comparison of the advantage and disadvantage of the epitaxial techniques are presented in **Table I.I**[20].

Table I.I

	LPE	**Hydride VPE**	**MOCVD**	**MBE**
Al alloys	capable	difficult	capable	capable
Range of growth rate (μ/min)	0.1 ~ 10	0.01 ~ 0.5	0.005 ~ 1.5	few ~ 0.05
Minimum thickness (Å)	500	250	20	5
Homogeneity	good	good	good	good
Surface morphology	bad	good	good	good
Abruptness of interface	bad	good	good	excellent
Doping level (cm^{-3})	10^{14} ~ 10^{19}	10^{14} ~ 10^{19}	10^{14} ~ 10^{19}	10^{14} ~ 10^{19}
Number of heating point	1	2	1	3
Productivity	low	high	high	very low

1.2.1 Metal-organic Chemical Vapor Deposition (MOCVD)

Among the all epitaxial growth techniques, MOCVD method represents the most promising technology for the growth of new compound semiconductor epitaxial layers due to the high growth rate with the accurate control over the composition of the compounds. The technique involves the reaction at a temperature well below the melting point of the resultant solid of two or more chemically reactive gases at atmospheric or reduced pressure. The epitaxial growth occurs in two steps : (1) decomposition and reaction of lower-order metal alkyl, such as trimethylgallium (TMG) mixed in the vapor phase with a hydride such as arsine (As_3H) and (2) growth of compound epitaxial layer on the heated single-crystal substrate. There are different growth mechanism involve in the growth of GaAs depending upon the substrate temperature : (1) At lower temperatures (< 550°C) the growth mechanism is surface kinetic limited, 2) between 550°C and 750°C mass transport is dominant and (3) at higher temperatures (> 800°C) it is governed by thermodynamics.

As a MOCVD source materials, the metal-organic sources must have two basic characteristics: (1) they must have suitable vapor pressure (~ 10 torr) at reasonable temperature (-20° to +20°), and (2) able to thermally decompose at typical growth temperatures to supply the desired group-III or group-V elements for the growth process[21].

1.3 Heteroepitaxial Growth of GaAs on Si

A combination of a GaAs-based compound semiconductor with highly doped Si has great potential for the creation of novel semiconductor materials which incorporate photonic functions such as light emission and high-speed operation into highly integrated Si-based electronic devices. For example, the growth of high quality, uniform, smooth layers of GaAs and AlGaAs on large-

diameter Si substrates would permit the realization of very-large-scale-integration (VLSI) of advanced GaAs integrated circuits as well as large area monolithic microwave integrated circuits (MMICs). In addition, the successful growth of reliable GaAs-based heteroepitaxial injection lasers, photodetectors, waveguides and modulators directly on Si would make possible the integration of Si electronics with high-speed, low-power opto-electronic functions and permit the fabrication of large-scale opto-electronic integrated circuits (OEICs). Even though the electronic and optical properties of GaAs are superior to those of Si, there are other technological benefits to be derived from the successful growth of GaAs on Si by gaining the GaAs device behavior with the better thermal and mechanical properties of Si together[22-29]. The heteroepitaxial system exploits the individual properties of the constituents to yield a highly optimized overall system. GaAs circuits fabricated on Si substrates can exhibit higher resistance to thermal burnout and runaway than those on GaAs substrates. Further to achieve the same mechanical strength as GaAs on Si, the GaAs on GaAs requires thicker substrates. Also the necessity of large GaAs wafer size for the MIMICs, VLSI, memory circuits, OEICs etc., and the shortage of growth technology may be satisfied if the realization of GaAs growth on Si becomes practical.

From the above mentioned considerations of GaAs/Si, the research to grow high quality GaAs/Si have attracted much interests[30-37]. However, the epitaxial growth of GaAs on Si is not without inherent problems. Among the many, the most important problems are (1) the growth initiation of polar (GaAs) semiconductor on a nonpolar (Si), (2) ~4% lattice mismatch and (3) ~250% difference in the thermal expansion coefficients between GaAs and Si[38].

Nonpolar semiconductors consist of a single atom, and both sub-lattices of the diamond structure are occupied by the same atom. Polar semiconductors consist of two (or more) atoms, and each atom resides in a particular sublattice. Epitaxial growth of polar semiconductors on nonpolar semiconductors often leads to structural defects known as antiphase boundaries (APBs) due to constituent

atoms occupying incorrect sublattices. Si and GaAs crystalline structures consist of two interpenetrating face centered cubic Bravais lattices. In the case of Si, the two f.c.c. lattices are the same. It is invariant to a rotation of $\pi/2$ and the [011] and $[01\bar{1}]$ directions are equivalent. In the case of GaAs, one f.c.c. lattice is occupied by Ga and the other by As, and the [111] and $[01\bar{1}]$ directions are not equivalent. This distinction is very visible in the (100) planes of GaAs (zinc-blend structure) which consist of alternating layers of gallium and arsenic. When GaAs is grown on GaAs substrate, the Ga and As atoms experience no ambiguity in choosing lattice sites, the epilayer just mimics the crystalline structure of the substrate. However, when epilayers of GaAs are grown on Si (100), Ga and As atoms can exhibit ambiguity in choosing lattice sites. The lattice sites on (100) planes are indistinguishable and so there are no preferential nucleation sites for Ga and As.

The formation of antiphase disorders in the GaAs epilayers is aided by monolayer high steps. Since the GaAs (100) planes alternate between cation and anion planes, the single steps cause a perturbation of the order of the (100) planes. However, the formation of antiphase domains (APDs) require large energies, and the inherent growth kinetics may not favor them. So, it is possible to grow APD free epilayers in spite of the presence of monolayer high steps and nonuniform initial monolayer on the surface. One way to solve this problem is to use of nominal (100) oriented Si substrate with a slight misorientation between 2 and 4° towards the [011] direction[47]. This effect is accomplished through the formation of a (100) Si surface with a large density of double atomic layer steps on the Si surface as a result of heat treatment of the misoriented Si substrate.

The lattice constant of GaAs is larger than that of Si. This mismatch causes strain on the lattice of the epilayer. The energy associated with the strain is proportional to the thickness of the epilayer[39]. If the thickness of the epilayer is smaller than the critical thickness the mismatch is accommodated by elastic deformation of the lattice, i.e., the GaAs lattice is compressed in the plane of the growth and expanded in the plane perpendicular to the plane of growth. When the

epilayers are thick, the associated strain energy is larger than the misfit dislocation energy. Then dislocations (~ $10^6/cm^2$) are generated to relieve strain energy[40]. Dislocations affect the quality of the epilayer in several different ways. Dislocations and other structural defects form nonradiative recombination centers. The number of these centers can be increased under photon fluxes, such as those in lasers.

The bulk thermal expansion coefficient of GaAs is $6.0\times10^{-6}/K$ and that of Si is $2.3\times10^{-6}/K$. Usually the growth is carried out at a high temperature. The strain caused by the lattice mismatch is relaxed by the generation of misfits and the GaAs epilayer is grown essentially stress free. Therefore, at the growth temperature, GaAs and Si maintain their own lattice parameters. As the structure is cooled from the growth temperature, the GaAs tries to contract more than Si substrate does, which lead to a high level of tensile stress (~10^9 dyn/cm^2) in the GaAs film together with significant warpage of the substrate[41].

As a result of both lattice mismatch and thermal mismatch high dislocation density at the hetero-interface is observed. Several reports stated, that the magnitude of such stress and dislocation density can greatly enhance the migration of dislocations and form the dark line defect (DLD) networks in the epitaxially grown devices[42-44]. A small fraction of these interfacial defects thread through into the GaAs epilayer, and this is the major drawback towards the application point of view. These dislocation networks are centers for no-radiative recombination, and believe to be responsible for the rapid degradation of opto-electronic devices grown on Si[38]. Certainly the major problems mentioned above have to be overcome in order to have an efficient utility in the device arena.

The effort in epitaxial growth of GaAs layers on Si substrates has steadily increased during the last several years and several approaches have been proposed to confine these misfit dislocations near the GaAs/Si interface[45-50]. The significant among the proposed methods are: (1) low temperature growth[45,46], (2) growth of a strained layer superlattice (SLS) buffer layer such as the InGaAs on

GaAs/Si[47], (3) the use of a orientation tilted Si substrate[47,48]. Thermal cycle annealing (TCA) also adopted in the growth of GaAs on Si in order to reduce the dislocation density[49]. Nozawa et al. have reported that the etch pit density (EPD) was drastically reduced to 7×10^4 cm^{-2} by a combination InGaAs/GaAs SLSs inserted into GaAs layers on Si[50]. The growth on the pre-patterned Si substrates is also useful for reducing the dislocation density[51-56]. Later, Chang et al.[57] reported the dislocation free GaAs epilayer on Si substrate using epitaxial lateral overgrowth (ELO) technique on a partially masked GaAs-coated Si and high quality devices are expected to be realized due to the demonstrated better quality epilayers.

1.4 GaAs-based Devices : Lasers on Si

In spite of the above mentioned problems, numerous GaAs-based electrical and optical devices, including field-effect transistors (FETs)[58], high electron mobility transistors (HEMTs)[59,60], modulators[61], waveguides[62], photodetectors[63], solar cells[64], LEDs[65] and lasers[66-71] have been fabricated on Si substrates by heteroepitaxy.

In 1984, Windhorn and coworker[66] were the first to report the successful growth of AlGaAs-GaAs DH injection lasers on Si substrate with a pulsed 77 K threshold current density of 10 kA/cm^2. But, for a semiconductor laser, quality laser must operate at room temperature under continuous wave (CW) operation. The presence of dislocations, strain and other defects present in the laser diode hinder the RT operation and also raise the threshold current densities[72]. The significant progress in the heteroepitaxial growth of laser diodes by molecular beam epitaxy (MBE) and metalorganic vapor phase epitaxy (MOVPE) led to substantial reduction in threshold current density of the laser diode on Si substrates[73,74]. Deppe et al.[75] and Chen et al.[76] reported the room temperature CW operation of lasers on Si substrates grown by MBE. However, most of the

interest has been focused on the realization of reliable long life time GaAs-based LEDs and lasers on Si because of needs for optical interconnects in future OEICs. Deppe et al. reported a lifetime of ~4.6 h under CW condition at RT and was increased to ~16 h by using microcracks for an AlGaAs/GaAs laser on Si[69,72]. In 1990, room temperature CW operation of an AlGaAs/GaAs laser on Si grown by MOCVD alone was achieved by Egawa et al.[70]. Choi et al.[71] reported the CW lifetime of ~56.5 h by replacing the GaAs active layer with a strained InGaAs layer. Furthermore, an AlGaAs/GaAs SQW laser on a sawtooth Si substrate was operated under room temperature CW condition for ~100 h[77].

Extensive research has been done in the last few years to understand the rapid degradation mechanism and develop the long-life reliable lasers. Egawa et al. reported the growth of <100> dark Line defects (DLDs) that originated from the threading dislocations, grew very rapidly with increasing injected current density, in an AlGaAs/GaAs laser on Si[78]. Hasegawa et al. reported suppression of the DLD growth in AlGaAs/GaAs laser on Si by the introduction of InGaAs intermediate layer[79].

Though several methods have been proposed to improve the reliability of GaAs-based lasers on Si, but the performance is still marginal. Growth of InAs self-organized quantum dots (QDs) in laser structure emerges as new approach to enhance the lasing efficiency and reliability of laser diodes[80,81]. InAs quantum dots sandwiched in GaAs based laser diode has an increasing research interest[82]. Egawa et al. have demonstrated AlGaAs/GaAs laser diodes on Si grown by "droplet" epitaxy with GaAs island-like active regions[83]. Later, K. K. Linder et al. reported the growth of self-organized $In_{0.4}G_{0.6}As$ quantum dot laser on Si substrates by MBE[84]. However, so far, no quantum dot laser structure was reported on Si substrate with RT continuous wave operation. The reason is supposed to be due to the non-uniform growth behavior of the dot size and lower density[85], which fails to enhance the quantum mechanical effect on the lasing action[86].

Further more, incorporation of In in the active region or in SLS layer leads to increase in non-radiative Auger recombination even though it retards the propagation of DLDs[87]. So, to realize the reliable laser on Si with QD active region the proper optimization of the QD size, density and In content is needed.

1.5 Purpose and Organization of Dissertation

As stated earlier, the stability of the laser diode can be improved by optimizing the In content in the SLS layer as well as in the active region with organized, equi-distributed, highly strained three dimensional islands or quantum dots in the active region[80,81]. Efforts were made to attain such superior quality laser diode structure by using atmospheric pressure metal organic chemical vapor deposition (AP-MOCVD) on the commercially available silicon substrates. The work done was resulted significant improvement in the laser operating time and emission characteristics.

The dissertation is composed of five chapters and each of them is summarized as follows,

Chapter 1 deals about the brief introduction about the chosen problem of the growth of GaAs based laser diodes on Si substrates and its present state of art.

In chapter 2, the operating characteristics such as internal quantum efficiency, internal loss, gain coefficient and transparency current density of the AlGaAs-GaAs lasers on Si are studied. Further, the temperature dependent characteristics and the time resolved photoluminescence investigations were carried out and discussed.

Chapter 3 deals about the optimization of InGaAs QD on Si using Stransky-Krastanov (S-K) growth mode, QD-like laser fabrication using a single layer $In_xGa_{1-x}As$ QD-like active region. Effect of different percentage of In incorporation on lasing characteristics were also studied.

Quality of Epitaxially over grown (ELO) GaAs on Si substrate using SiO_2 growth window is presented in chapter 4 together with standard test samples. Suitability of ELO layer quality for laser diode fabrication was analyzed by fabricating laser diodes.

The achievements of the work is summarized and suggestions for the future work is presented in Chapter 5.

References

1. J. Bardeen and W. H. Brattain, Phys. Rev., **74**, 230 (1948).
2. H. Morkoc, H. Unlu, H. Zabel, N. Otsuka, Solid State Tech., **31**, 71 (1988).
3. W. Welker, Z. Naturforsh, **11**, 1744 (1952).
4. J. I. Pankove, Phys. Rev. Lett., **9**, 283 (1962)
5. J. I. Pankove and J. E. Berkeyheiser, Proc. I. R. E., **50**, 1976 (1962).
6. D. N. Nasledov, A. A. Rogachev, S. M. Ryvkin and B. V. Tsarenkov, Fiz. Tverd. Tela., **4**, 1062 (1962).
7. R. N. Hall, G. E. Fenner, J. D. Kingsley, T. J. Soltys and R. O. Carlson, Phys. Rev. Lett., **9**, 366 (1962).
8. R. D. Dupuis and P. D. Dapkus, Appl. Phys. Lett., **32**, 406 (1978).
9. R. R. Saxena, V. Aebi, C. B. Cooper III, M. J. Ludowise, H. A. Vander Plas, B. R. Carins, T. J. Maloney, P. G. Borden and P. E. Gregory, Appl. Phys. Lett., **51**, 4501 (1980).
10. T. Nakanishi, T. Udagawa, A. Tanaka and K. Kamei, J. Cryst. Growth, **55**, 255 (1981).
11. V. K. Jain and S. K. Sharma, Solid State Electron., **13**, 1145 (1970).
12. J. J. Heish, Liquid phase epitaxy, in Handbook on Semiconductor, vol. **3**, pp. 415-497, ed. by S.P. Keller, North-Holland (1980).
13. M. B. Panish and A. Y. Cho, IEEE Spectrum, **18** (April 1983).
14. H. M. Manasevit, J. Cryst. Growth, **55**, 1 (1981).
15. H. J. Scheel, Appl. Phys. Lett., **37**, 70 (1980).
16. A. Y. Cho, J. Vac. Sci. Tech., **16**, 275 (1979).
17. W. G. Herrenden-Harker and R. H. Williams, *Epitaxial Growth of GaAs: MBE and MOCVD*, p. 57, ed. by H. Thomas, D. V. Morgan, B. Thomas, J. E. Aubrey and G. B. Morgan, IEE UWIST (1985).

18. E. Johnson, R. Tsui, D. Convey, N. Meller and J. Curless, J. Cryst. Growth., **69**, 497 (1984).

19. P. D. Dapkus., J. Cryst. Growth, &8, 345 (1984).

20. L. P. Chen., Ph. D. Dissertation, National Cheng Kung University, Taiwan (1987).

21. G. B. Stringfellow, *Semiconductors and Semimetals*, vol. **22**, p. 209, ed. by W. Tsang, Academic Press (1985).

22. W. I. Wang, Appl. Phys. Lett., **44**, 1149 (1984).

23. B. Y. Tsaur and G. M. Metze, Appl. Phys. Lett., **45**, 535 (1984).

24. S. M. Vernon, V. E. Haven, S. P. Tobin and R. G. Wolfson, J. Cryst. Growth, **77**, 530 (1986).

25. S. K. Shastry and S. Zemon, Appl. Phys. Lett., **49**, 467 (1986).

26. R. Fischer, H. Morcok, D. Neumann, H. Zabel, C. Choi, N. Ohtsuka, M. Longerbone and L. P. Erikson, J. Appl. Phys., **60**, 1640 (1986).

27. W. M. Duncan, J. W. Lee, R. J. Matyi and H. Y. Lui, J. Appl. Phys., **59**, 2161 (1986).

28. S. J. Rosner, S. M. Koch and J. S. Harris, Jr., Appl. Phys. Lett., **49**, 1764 (1986).

29. K. Ishida, M. Akiyama and S. Nishi, Jpn. J. Appl. Phys., **26**, L163, (1987).

30. H. K. Choi, J. P. Mattia, G. W. Turner and B. Y. Tsaur, IEEE Electron Device Lett., **9**, 512 (1988).

31. H. Shichijo, R. Matyi, A. H. Taddiken and Y. C. Kao, IEEE Trans. Electron Devices, **37**, 548 (1990).

32. T. Egawa, T. Jimbo and M. Umeno, IEEE Photonic Technol. Lett., **4**, 612 (1992).

33. T. Egawa, T. Jimbo and M. Umeno, IEICE Trans. Electron., **E76-C**, 106 (1993).

34. G. N. Nasserbakht, J. W. Adkisson, B. A. Wooly, J. S. Harris and T. I.

Kamis, IEEE J. Solid-State Circuits, **28**, 622 (1993).

35. I. Hayashi, Jpn. J. Appl. Phys., **32**, 266 (1993).
36. I. Hayashi, Optoelectron. Devices Technol., **9**, 468 (1994).
37. K. W. Goossen, J. A. Walker, L. A. D'Asaro, S. P. Hui, B. Tseng, R. Leibenguth, D. Kossives, D. D. Bacon, D. Dahringer, L. M. F. Chirovsky, A. L. Lentine and D. A. B. Miller, IEEE Photon. Technol. Lett., **7**, 360 (1995).
38. H. B. Kroemer, Proc. Mater. Res. Soc., **67**, 3 (1986).
39. R. People and J. C. Bean, Appl. Phys. Lett., **47**, 322 (1985).
40. R. D. Dupuis and C. J. Pizone, J. Cryst. Growth, **93**, 435 (1988).
41. W. D. Nix, Metall. Trans., **20A**, 2217 (1989).
42. R. L. Hartman and A. R. Hartman, Appl. Phys. Lett., **23**, 147 (1973).
43. T. Kamejima, K. Ishida and J. Matsui, Jpn. J. Appl. Phys., **16**, 233 (1977).
44. A. R. Goodwin, P. A. Kirkby, I. G. Davies and R. S. Baulcomb, Appl. Phys. Lett., **34**, 647, (1979).
45. M. Akiyama, Y. Kawarada and K. Kaminishi, Jpn. J. Appl. Phys., **23**, L843 (1984).
46. W. T. Masselink, T. Henderson, j. Klem, R. Fischer, P. Pearah, H. Morcok, M. Hafich, P. D. Wang and G. Y. Robinson, Appl. Phys. Lett., **45**, 1309 (1984).
47. R. Fischer, D. Neuman, H. Zabel, H. Morcok, C. Choi and N. Otsuka, Appl. Phys. Lett., **48**, 1223 (1986).
48. G. M. Metze, H. K. Choi and B. Y. Tsaur, Appl. Phys. Lett., **45**, 1107 (1984).
49. M. Yamaguchi, M. Sugo, Y. Ito, Appl. Phys. lett., **54**, 2568 (1989).
50. K. Nozawa and Y. Hirokoshi, Jpn. J. Appl. Phys., **30**, L668 (1991).
51. K. Ismail, F. Legoues, N. H. Karam, J. Carter and H. I. Smith, Appl. Phys. Lett., **59**, 2418 (1991).

52. K. R. Sprung, K. Wilke, G. Heymann, J. Varrio and M. Pessa, Appl. Phys. Lett., **62**, 2711 (1993).

53. R. Murray, C. Roberts, K. Woodbridge, P. barnes, G. Parry and C. Norman, Appl. Phys. Lett., **62**, 2929 (1993).

54. J. G. Zhu, M. M. Al-Jassim, N. H. Karam and K. M. Jones, *Mat. Res. Soc. Symp. Proc.*, **281**, 327 (1993).

55. A. krost, R. F. Schnabel, F. Heinrichsdorff, U. Rossow, D. Bimberg and H. Cerva, J. Cryst. Growth, **145**, 314 (1994).

56. J. Knall, L. T. Romano, D. K. Biegelsen, R. D. Bringans, H. C. Chui, J. S. Harris, Jr., D. W. Treat and D. P. Bour, J. Appl. Phys., **76**, 2697 (1994).

57. Y. S. Chang, S. Naritsuka, T. Nishinaga, J. Cryst. Growth, **192**, 18 (1998).

58. T. Egawa, S. Nozaki, T. Soga, T. Jimbo and M. Umeno, Appl. Phys. Lett., **58**, 1265 (1991).

59. T. Aigo, A. Jono, A. Tachikawa, R. Hiratsuka and A. Moritani, Appl. Phys. Lett., **64**, 3127 (1994).

60. T. Ohori, H. Suehiro, K. Kasai and J. Komeno, Jpn. J. Appl. Phys., **33**, 4499 (1994).

61. K. W. Goossen, G. D. Boyd, J. E. Cunningham, W. Y. Jan, D. A. B. Miller, D. S. Chemla and R. M. Lum, IEEE Photon. Tech. Lett., **1**, 304 (1989).

62. T. Yuasa, Y. Nagashima, T. Murase, T. Jimbo and M. Umeno, Jpn. J. Appl. Phys., **32**, L1055 (1993).

63. J. Paslasky, H. Z. Chen, H. Morcok and Y. Yariv, Appl. Phys. Lett., **52**, 1410 (1988).

64. M. Yang, T. Soga, T. Jimbo and M. Umeno, Jpn. J. Appl. Phys., **33**, 6605 (1994).

65. N. Wada, S. Sakai and M. Fukui, Jpn. J. Appl. Phys., **33**, 864 (1994).

66. T. H. Windhorn, G. M. Metze, B. Y. Tsaur and J. C. C. Fan, Appl. Phys. Lett., **45**, 309 (1984).

67. T. H. windhorn, G. w. turner and G. M. Metze, *Mat. Res. Soc. Proc.*, **67**, 157 (1986).

68. S. Sakai, T. Soga, M. Takeyasu and M. Umeno, Appl. Phys. Lett., **48**, 413 (1986).

69. D. G. Deppe, D. W. Nam, N. Holonyak, Jr., K. C. Hsie, R. J. Matyi, H. Shichijo, J. E. Epler and H. F. Chung, Appl. Phys. Lett., **51**, 1271 (1987).

70. T. Egawa, H. Tada, Y. Kobayashi, T. Soga, T. Jimbo and m. Umeno, Appl. Phys. Lett., **57**, 1179 (1990).

71. H. K. Choi, C. A. Wang and N. H. Karam, Appl. Phys. Lett., **59**, 2634 (1991).

72. D. G. Deppe, D. C. Hall, N. Holonyak, jr., R. J. Matyi, H. Shichijo and J. E. Epler, Appl. Phys. Lett., **53**, 874 (1988).

73. R. Fischer, W. Kopp, H. Morkoc, M. Pion, A. Specht, G. Burkhart, H. Appelman, D. McGougan and R. Rice, Appl. Phys. Lett., **48**, 1360 (1986).

74. P. van der Ziel, R. D. Dupuis, r. A. Logan, R. M. Mikulyak, C. J. Pinzone and A. Savage, Appl. Phys. Lett., **50**, 454 (1987).

75. D. G. Deppe, N. Holonyak, D. W. Nam, K. C. Hsieh, G. S. Jackson, R. J. Matyi, H. Shichijo, J. E. Epler and H. F. Chung, Appl. Phys. Lett., **51**, 637 (1987).

76. H. Z. Chen, A. Ghaffari, H. Wang, H. Morkoc and A. Yariv, Appl. Phys. Lett., **51**, 1320 (1987).

77. J. De Boeck and G. Borghs, J. Cryst. Growth, **127**, 85 (1993).

78. T. Egawa, Y. Hasegawa, T. Jimbo and M. Umeno, Appl. Phys. Lett., **67**, 2995 (1995).

79. Y. Hasegawa, T. Egawa, T. Jimbo and M. Umeno, Jpn. J. Appl. Phys.,

35, 5637 (1996).

80. L. Goldstein, F. Glas, J. Y. Marzin, M.N. Charase and G. Leroux, Appl. Phys., Lett., **47**, 1099 (1985).
81. P. R. Berger, K. Chang, P. Bhttacharya, J. Singh and K. K. Bajaj, Appl. Phys. Lett., **53**, 684 (1988).
82. J. M. Gerard, O. Cabrol and B. Sermage, Appl. Phys. Lett., **68**, 3123 (1996).
83. T. Egawa, A. Ogawa, T. Jimbo and M. Umeno, Jpn. J. Appl. Phys., **37**, 1552 (1998).
84. K. K. Linder, J. Philips, O. Qasaimeh, X. F. Liu, S. Krishna, P. Bhattacharya, J. C. Jiang, Appl. Phys. Lett., **74**, 1355 (1999).
85. E. P. O'Reilly, Semicond. Sci. Tech., **4**, 121 (1989).
86. H. Shoji, K. Mukai, N. Ohtsuka, M. Sugawara, T. Uchida and H. Ishikawa, IEEE Photon. Tech. Lett., **7**, 1385 (1995).
87. S. F. Fang, K. Adomi, S. Iyer, H. Morkoc, H. Zabel, C. Choi and N. Otsuka, J. Appl. Phys., **68**, R31 (1990).

Growth and Characterization of AlGaAs/GaAs/Si Laser Diodes with GaAs Islands Active Region Using Droplet Epitaxy

2.1 Introduction

Quantum confinement of charge carriers in more than one-dimension can be achieved by fashioning lateral potential wells of sufficiently small lateral extent. Quantum confinement in one or both lateral dimensions can lead to quasi-1D or 0D carriers trapped in quantum wire (QWR) or quantum dot (QD) heterostructures. The reduced dimensionality in these structures results in significant modification in the density of states (DOS) profile, which acquires increasingly sharp features at the bound state energies as the dimensionality is reduced. This in turn, is expected to give rise to a variety of new physical effects, including modified optical absorption, refraction[1] and gain spectra[2], enhanced exciton and impurity binding energies[3,4] and reduced carrier scattering rates[5]. These effects should be useful in enhancing the performance of lasers[2,6] by resulting highly monochromatized light, low threshold current density, reduced temperature sensitivity and improved spectral characteristics due to a reduced line-width enhancement factor[7-10].

Many techniques have been proposed in order to fabricate the QD structures, such as, electron beam lithography[11], selective growth on masked substrate[12], Stransky-Krastanov growth mode[13], droplet epitaxy[14] and so on. Droplet epitaxy is proved as promising method for fabricating QDs[15]. In the droplet epitaxy, the column III metal forms the droplet on the substrate and subsequent column V atoms transform the droplet into single crystals by reacting the droplets. As mentioned earlier that the GaAs-based laser diodes on Si suffering from rapid degradation due to the large number of dislocations and it is

believed that the inclusion of self assembled islands in the active region improve the reliability.

The self-formed nanometer-scale GaAs and InGaAs quantum dot-like islands have been realized using droplet epitaxy[16] and the lasers with these islands in the active regions have been also fabricated[17].

In this chapter, the fabrication of GaAs based laser diodes with AlGaAs barrier layer and self-formed GaAs island active region is discussed. The total laser structure is fabricated by MOCVD. Droplet epitaxial technique by MOCVD method is used to realize GaAs islands. Different optical and thermal characteristics of the laser diode were studied and the results are discussed in detail.

2.2 Experimental

2.2.1 MOCVD Growth of Laser Diode

Before the epitaxial growth, the Si substrates were cleaned by acetone and methanol respectively using ultrasonic bath. Prior to loading for deposition, the substrates were etched by H_2SO_4:H_2O_2 (4:1) solutions for 4 minutes and by HF:H_2O (1:1) solutions for one minute. Finally one minute etching was done by HCl.

The laser structures were grown on the (100) n^+-Si substrates oriented 2° off towards the [011] direction using rf-heated horizontal metal organic chemical vapor deposition (MOCVD) reactor at atmospheric pressure. Trimethylgallium (TMG) and trimethylaluminum (TMA) were chosen as group-III sources and arsine (AsH_3) was chosen as the group-V source. Hydrogen selenide (H_2Se) and diethylzinc (DEZ) were injected as the n- and p-dopants, respectively. Hydrogen was used as the carrier gas.

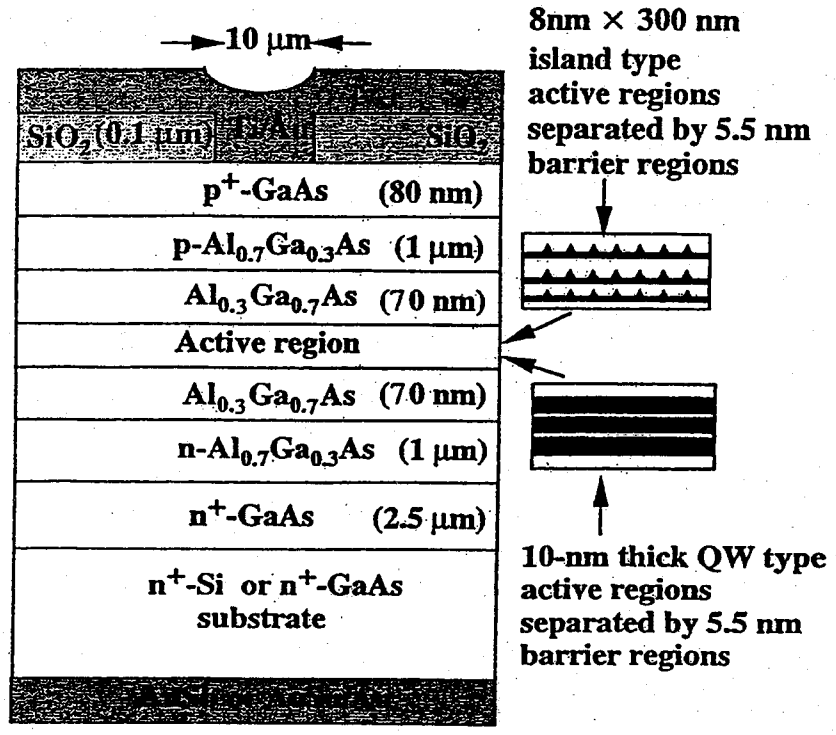

Figure 2.1 : Schematic structure of the MOCVD-grown AlGaAs-GaAs laser diode. Two types of active regions are shown adjacent to the structure.

The loaded silicon substrates were pre-heated 10 minutes at 1000°C in order to remove the native oxide layer then the substrate temperature was lowered to 400°C. An initial 10-nm thick undoped GaAs nucleation layer was deposited at 400°C using TMG and AsH_3 sources of 10 sccm and 34.6 sccm respectively. Further, the growth temperature was raised to 750°C and 2.5 μm thick n^+-GaAs buffer layer (Se-doped, 2×10^{18} cm^{-3}) was grown at 750°C by re-fixing the gas composition as 10 sccm of TMG, 17.3 sccm of AsH_3 and 45 sccm of H_2Se. During the growth of the n^+-GaAs buffer layer, the substrate temperature was cycled five times from 350 to 850° C in an AsH_3 atmosphere in order to reduce the threading dislocation in the GaAs layer[18]. The 1.0 μm thick n-$Al_{0.7}Ga_{0.3}As$ lower cladding layer (TMG: 3 sccm, TMA: 16.3 sccm, AsH_3: 17.3 sccm, H_2Se: 55 sccm), a 70 nm thick undoped $Al_{0.3}Ga_{0.7}As$ lower confining layer (TMG: 9.1 sccm, TMA: 7.8 sccm, AsH_3: 27.8 sccm), active regions separated by 5.5 nm thick undoped $Al_{0.3}Ga_{0.7}As$ barrier layers (TMG: 9.1 sccm, TMA: 7.8 sccm, AsH_3: 27.8 sccm), 1.0 μm thick p-$Al_{0.7}Ga_{0.3}As$ (Zn-doped, 1×10^{18} cm^{-3}) upper cladding layer (TMG: 3 sccm, TMA: 16.3 sccm, AsH_3: 34.6 sccm and DEZ: 8 sccm) and an 80 nm thick p^+-GaAs (Zn-doped, 1×10^{18} cm^{-3}) contact layers (TMG: 9.1 sccm, AsH_3: 17.3 sccm, DEZ: 20 sccm) were grown in order to realize the laser diode structure as shown in Fig. 2.1.

2.2.2 MOCVD Growth of GaAs Islands by Droplet Epitaxy

After the growth of laser diode structure up to the lower confining layer of $Al_{0.3}Ga_{0.7}As$, GaAs islands were grown by the droplet epitaxial technique in the following manner: after, attaining the substrate temperature to 700°C, the AsH_3 flow was stopped and TMG was supplied for six seconds to form the Ga droplets, immediately after AsH_3 was supplied again with five second interval and the Ga droplets were transformed to GaAs islands by inducing the reaction between As and Ga droplets. Upon the droped islands, further growth was continued to

complete the laser diode structure. The growth behavior of the GaAs islands were studied on GaAs/Si substrate prior to the application to the fabrication of laser diodes.

2.2.3 Processing to Laser Diodes

After the growth, the laser devices were processed as follows: A 0.1 μm thick SiO_2 insulating layer was deposited on the p^+-GaAs contact layer and 10 μm wide stripe contact windows were opened with a 300 μm pitch along the <110> direction by chemical etching ($HF:NH_4F:CH_3COOH$ = 1:20:7) of SiO_2. Then Ti/Au (50/150 nm) contacts were deposited by e-beam evaporation on the p^+-GaAs layer. After thinning the n^+-Si substrate to a thickness of 100 μm, AuSb/Au (50/150 nm) were deposited on the Si substrate in order to form the n-side electrode. The contacts were annealed in N_2 atmosphere at 380°C for 30 seconds in order to form the ohmic contact of the deposited metal electrodes. The samples were cleaved into chips with a desired cavity length (120-900 μm) and mounted on In-soldered Cu heat-sinks in the p-side-up configuration.

2.2.4 Characterization Studies

Atomic force microscope (AFM) measurements were carried out to characterize the island size and density. Injected current vs. output current (*I-L*) characteristics and emission spectrum analysis were carried out to observe the lasing property of the laser diode. Automatic current controlled (ACC) lifetime measurement and electroluminescence (EL) topograph have been performed in order to know the degradation mechanism of laser diodes.

2.3 Results and Discussion

2.3.1 Characteristics of GaAs Islands

The island structures in the active region are confirmed by AFM measurements. It was observed that the islands aligned on the cracks of GaAS/Si. The GaAs islands exhibited a conical shape with heights of 8 nm and diameter of 300 nm with a density of around 1~2 $\times$ 10^7 cm^{-2}. The observed island density resembles the density of etch pits presents in the GaAs on Si (10^7 cm^{-2})[17]. The sizes of the self-formed GaAs islands can be controlled by changing the growth conditions, such as the TMG flow time and rate[17]. At a fixed flow rate of 10 sccm, the island height increases from 8 nm to 330 nm with the increase in flow time from 3 sec to 9 sec. It is also observed that the island diameter increased from 250 to 300 nm. The island density was observed as constant at 1.5 $\times 10^7$ cm^{-2}, but the increase in TMG flow rate from 2 to 20 sccm, increased the island density from 4 $\times 10^6$ to 3 $\times 10^7$ cm^{-2}. The observation of increase in island density with the increase in flow rate reveals the importance over the control of TMG flow rate. However, such increase in island density is limited to the flow rate of 20 sccm and further increase saturated the island density[17].

2.3.2 Characteristics of Laser Diodes

The injected current versus light output (*I-L*) characteristic and emission spectrum of the self-formed laser diode on Si substrate under continuous wave (CW) operation at 100 K is shown in Fig. 2.2. The device resulted the threshold current density (J_{th}) of 3.9 kA/cm^2, with an external differential quantum efficiency (η_d) of 7%. The lasing behaviour was observed at a wavelength of 771 nm with the full width at half maximum (FWHM) of 1.8 nm. However, the device didn't result any CW lasing behavior at room temperature (RT). The same device

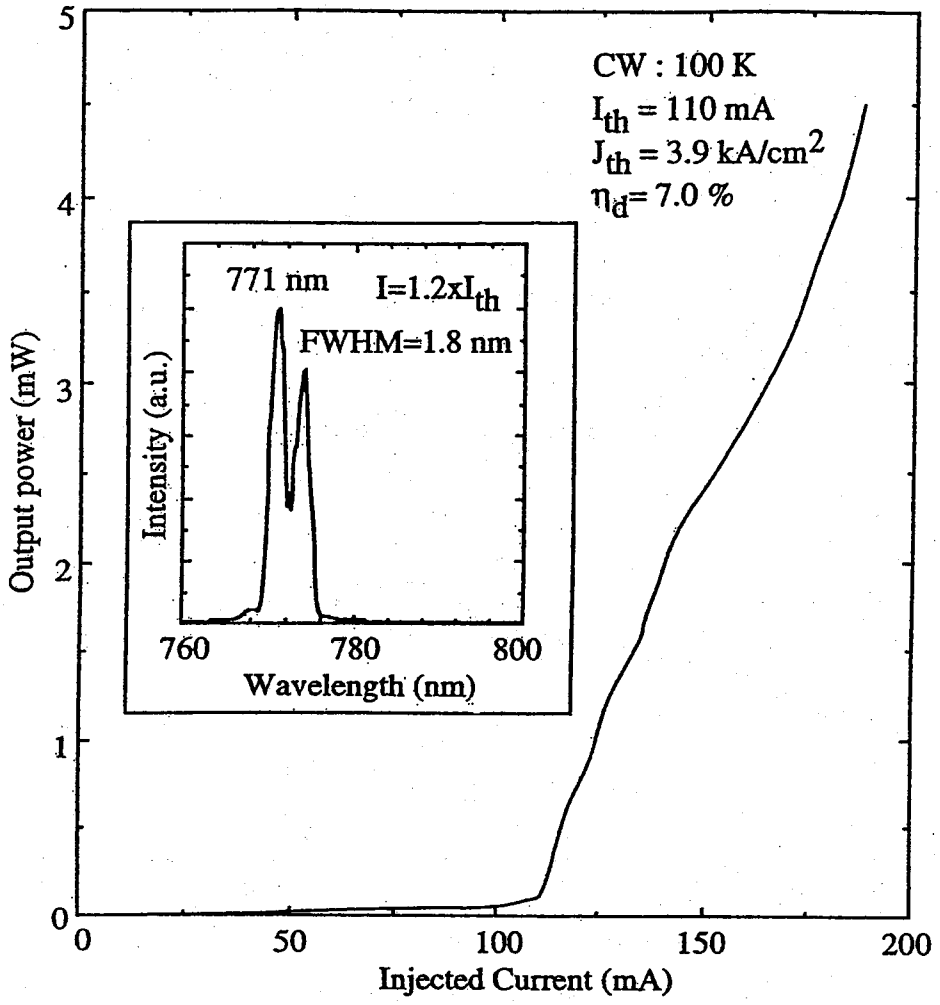

Figure 2.2 : *L-I* characteristic and emission spectrum of the AlGaAs-GaAs laser diode with the self-formed GaAs islands active regions on the Si substrate under cw condition at 100 K.

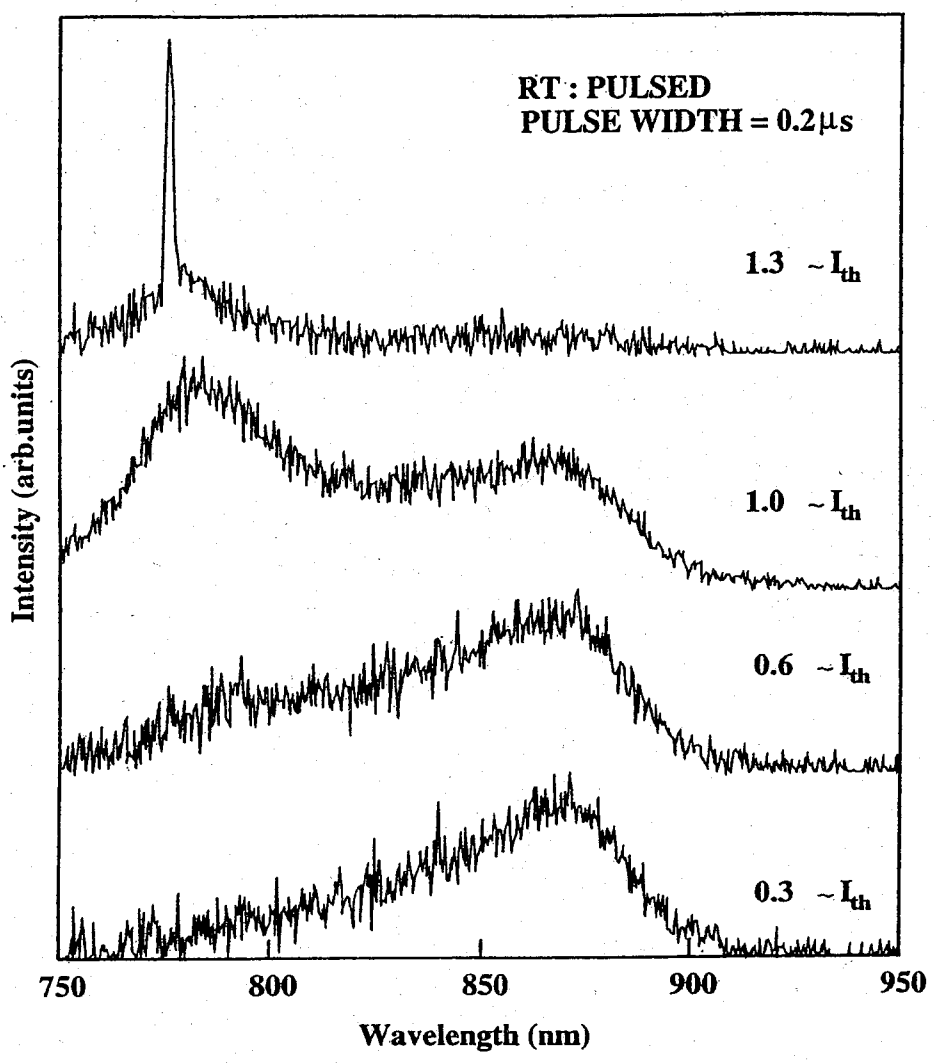

Figure 2.3 : Emission spectra of the GaAs island laser on Si substrate at different injected currents. Photon emission gradually transforms from ground state to secondary state as the injected current increases.

under pulsed conditions, exhibits the J_{th} of 5.4 kA/cm^2 with the η_d of 4.7% at 776 nm with the FWHM of 2.8 nm at 300 K. The lasing wavelengths of 771 nm and 776 nm, obtained under CW and pulsed conditions, are shorter than the reported 851 nm for the conventional quantum well laser on Si[18]. This point is illustrated in Fig. 2.3, which shows the emission spectra of the self-formed GaAs island laser on Si for different applied current density at RT under pulsed condition. It can be seen from the figure that, well below the threshold current density, the photon emission occurs from the ground state. However, as the injected current increases, the emission is gradually transfered from the ground state to the secondary state and at high injected current, ground state emission becomes negligible[19].

The external differential quantum efficiency η_d can be obtained from the *I-L* measurement by calculating the slope of the extrapolated line to x - axis zero. Since the cavity length of the laser is constant for each measurement, the following relation is used to calculate the η_i and α_i [20],

$$\frac{1}{\eta_d} = \frac{1}{\eta_i}[1 + \alpha_i L / \ln(1/R)] \qquad (1)$$

where R - is the mirror reflectivity and L - is the cavity length.

Further, the experimentally calculated η_d for the lasers with different cavity length is used to plot $1/\eta_d$ against the cavity length in Fig. 2.4. The calculations were carried out for both self-formed GaAs island lasers and conventional quantum well (QW) lasers at RT under pulsed condition. For a comparison, the same is plotted for the conventional QW laser on GaAs substrate. The η_i and α_i are obtained from the intercept of the vertical axis and the slope of the line, respectively. For the GaAs island laser on Si substrate, the value of η_i and α_i are found to be 62.4% and 16.2 cm^{-1}, with the value of R as 0.32, whereas for the conventional QW laser these are 59.4% and 28 cm^{-1}, respectively. The value of η_i is increased and the value of α_i is reduced in the case of island lasers.

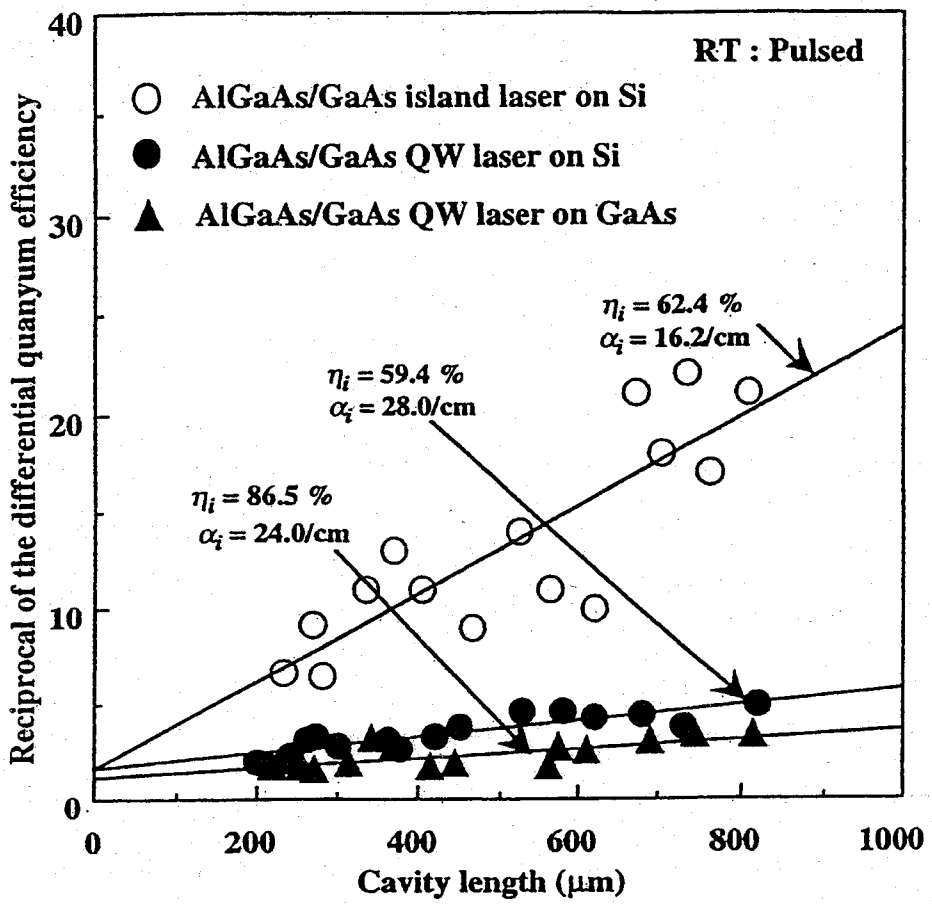

Figure 2.4 : Comparison of the reciprocal of the quantum efficiency vs. cavity length of self-formed GaAs TSI and conventional GaAs TQW laser on Si under pulsed condition at room temperature.

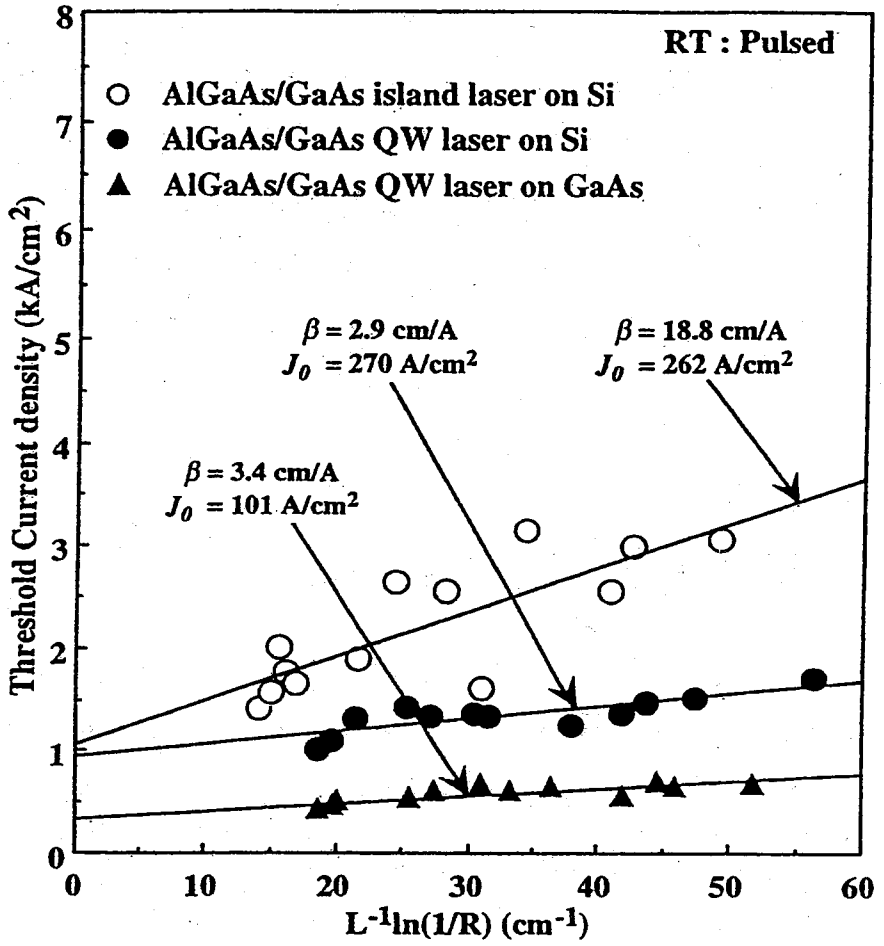

Figure 2.5 : Variation of the threshold current density with respect to cavity length of self-formed GaAs TSI and conventional GaAs TQW laser on Si under pulsed condition at room temperature.

Furthermore, the threshold current density J_{th} is related to β and J_0 as given in the following[21]:

$$J_{th} = J_0 / \eta_i + (\eta_i \beta \Gamma)^{-1} [\alpha_i + L^{-1} \ln(1/R)] \quad (2)$$

where Γ is the optical confinement factor. The confining factor is defined as the ratio of the light intensity within the active region to the sum of light intensity both within and outside the active region. In the case of conventional QW active regions, to evaluate the confining factor is easier, but in the case of island-type active regions this is more complicated. Here, a model is considered where the light emission is assumed to occur only from the island regions other than then whole active region. According to this consideration, the value of Γ must be dependent on the island density of the active region.

For the multiple-quantum-well laser, the effective refractive index $\bar{n}$ is given by[22]

$$\bar{n} = \frac{N_a t_a n_a + N_b t_b n_b}{N_a t_a + N_b t_b} \quad (3)$$

where N_a and N_b are the numbers of active and barrier layers respectively, whereas t_a and t_b are their thickness and n_a and n_b are their refractive indices. To calculate Γ of the island type lasers, the island size and density is considered here. For the island type laser the effective refractive index is modified as

$$\bar{n} = \frac{N_a t_a n_a V_i + N_a t_a n_b (1 - V_i) + N_a t_w n_a + N_b t_b n_b}{N_a t_a + N_b t_b} \quad (4)$$

where V_i denotes the fractional volume of active region contained islands only and t_w is the thickness of the wetting layer.

According to the refractive index technique the confining factor Γ is defined as[23]

$$\Gamma = \frac{\bar{D}^2}{\bar{D}^2 + 2} \quad (5)$$

where

$$\overline{D} = (2\pi\bar{t}/\lambda)(\bar{n}^2 - n_c^2)^{1/2}\,, \tag{6}$$

here, $\bar{t} = N_a t_a + N_b t_b$, λ is the emission wavelength peak of the laser and n_c is the refractive index of the cladding layer. Using the effective refractive index model the value of Γ of the QW laser is estimated as 0.0476. The island density of 2 $\times 10^7$ cm^{-2} with a height of 8 nm, diameter of 300 nm and wetting layer thickness 2 nm the value of Γ is found to nearly 0.002.

Figure 2.5 shows the variation of J_{th} with cavity length of the self-formed GaAs island laser and conventional QW laser on Si substrate at RT under pulsed condition. Using the relation (2), β and J_0 can be calculated. The value of β and J_0 of GaAs island laser on Si are found to be 18.8 cm/A and 262 A/cm^2 whereas for the conventional QW laser on Si these are 2.9 cm/A and 270 A/cm^2, respectively. Similarly, for the conventional QW laser on GaAs these are 3.4 cm/A and 101 A/cm^2, respectively. There is no remarkable change in J_0 for the island laser on Si compared to the QW laser on Si because of the presence of the free carriers in the adjacent regions of the islands, such that recombination in these regions gives rise to one more component of the threshold current.

For the laser diode lower threshold current is expected. But, the lasers with island type or quantum dot active regions suffer from the higher threshold current density[24]. It is suggested strongly that the lower confining factor of the laser is responsible for the higher threshold current density of the island type or quantum dot lasers. By increasing the confining factor one can reduce the threshold current density. One way to increase the confining factor is to increase the island/dot density in the active region.

2.3.3 Temperature Dependent Characteristics

Many factors such as the gain-current relationship, the degree of radiation and carrier confinement, internal absorption coefficient and the internal quantum efficiency influences on the temperature dependence of threshold current

characteristics[25-28]. Simplifying the variation of the complex combination of parameters such as temperature (T) dependence of the threshold current (I_{th}) of the diode laser is described by the Pankove relation[29]

$$I_{th} = I_0 \exp(T/T_0) \tag{7}$$

where I_0 is the threshold current extrapolated at $T = 0$, called the characteristic current and T_0 is the characteristic temperature of the device. Usually T_0 is a constant for a particular device. A higher value of T_0 implies that I_{th} is less sensitive to temperature. Temperature dependent characteristics of a number of GaAs island lasers on Si under CW condition has been made for a temperature range from 50 K to 150 K. Figure 2.6 shows a typical plot of the threshold current vs. temperature of the GaAs island laser and QW laser on Si substrate. In the whole temperature range, the threshold current density of GaAs island laser is higher than that for GaAs QW laser. Further, in the temperature range 50 - 100 K, the threshold current density varies relatively weakly and as a result the characteristic temperatures T_0's reveals higher value such as 198 K and 230 K respectively. Above 100 K, the threshold current increases sharply, causing lower characteristic temperatures. This is perhaps due to the fact that at higher temperature, the carriers present in the active region encounter thermal evaporation into the adjacent $Al_{0.7}Ga_{0.3}As$ layer by necessitating higher injection current density in order to maintain the given gain.

Moreover, GaAs island lasers show comparatively higher characteristic temperatures than those of QW laser (fig. 2.6), which means that the active region with GaAs island is less sensitive to temperature than that of conventional GaAs quantum well laser on Si substrate.

Further more, the temperature dependent external differential quantum efficiency measurement on both the GaAs island and QW laser exhibits the correlation to the following equation[29]

$$\eta = \eta_o \exp(-T/T_o) \tag{8}$$

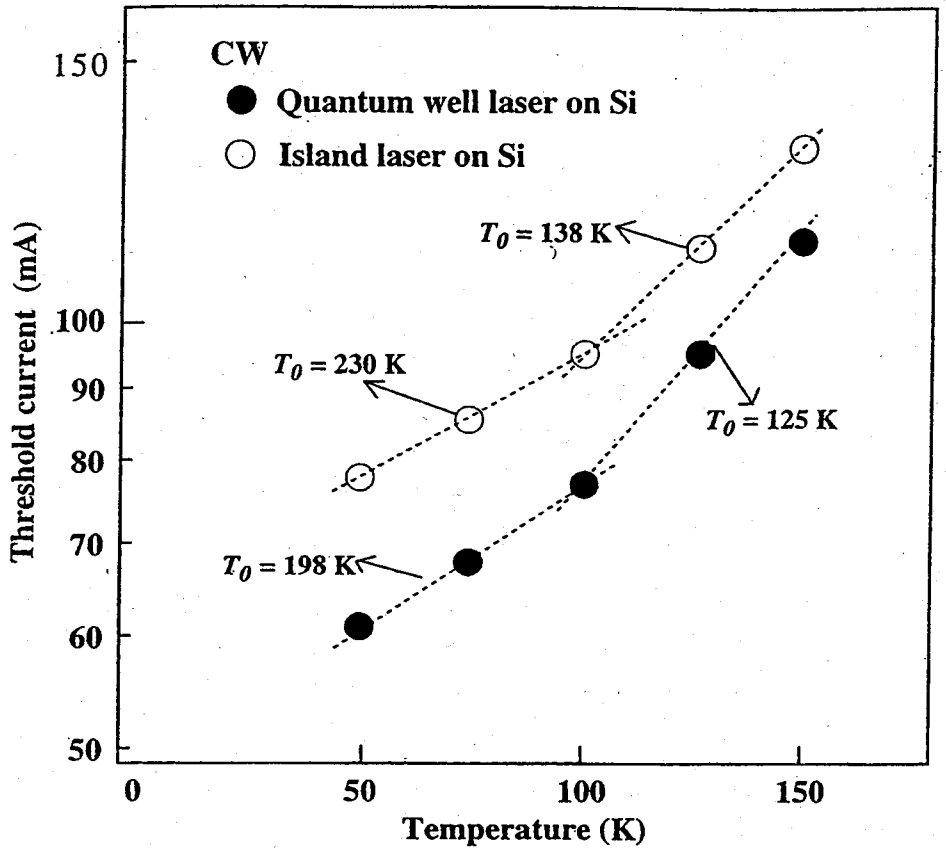

Figure 2.6 : Typical plots of threshold current vs. temperature for both self-formed GaAs TSI laser and conventional TQW laser on Si.

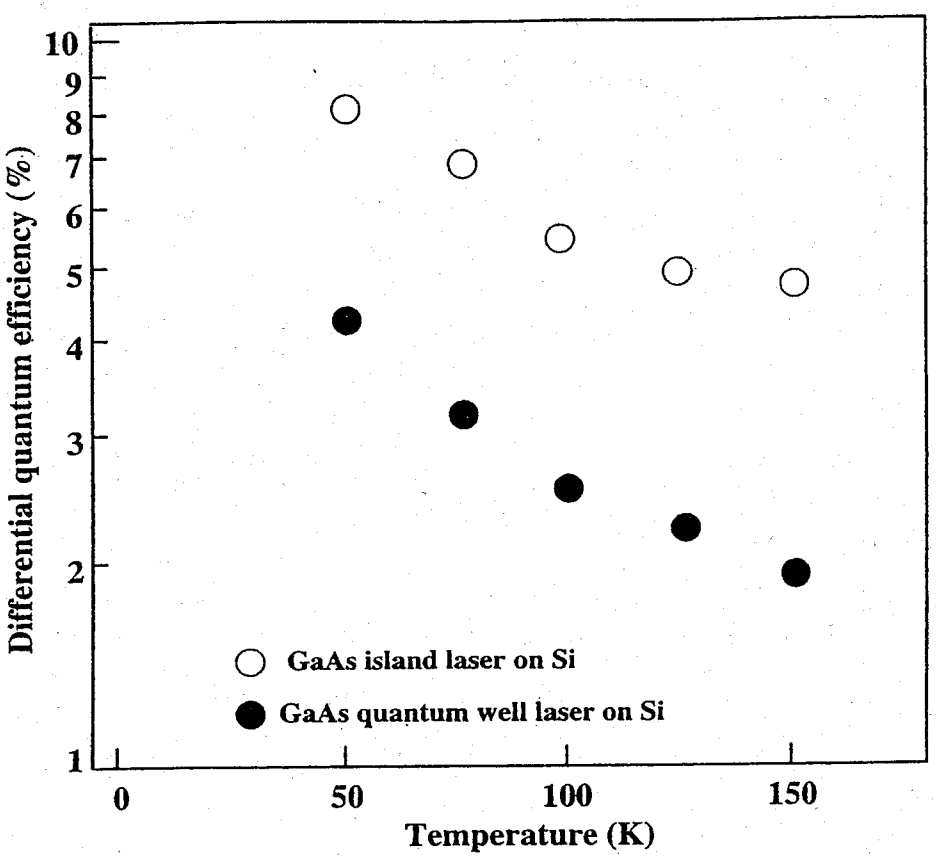

Figure 2.7 : Typical temperature dependence of the differential quantum efficiency of both self-formed GaAs TSI laser and conventional TQW laser on Si.

where η_0 is the external differential efficiency extrapolated to $T = 0$, and T_0 is the temperature coefficient same as stated in eq. (7).

Figure 2.7 shows the temperature dependence of the external differential quantum efficiency of GaAs island laser on Si substrate. It is found that the external quantum efficiency of both the lasers decreases as the temperature increases according to eqn. (8). However, the GaAs island laser exhibits always higher efficiency than the conventional QW laser for the whole temperature range. This is due to the lower confinement factor of island laser than the QW laser, which provides higher gain coefficient with higher external quantum efficiency.

The observed comparatively higher quantum efficiency at low temperature for both the island and conventional QW lasers are due to the thermal distribution of carrier population in the narrow subband ground state levels at relatively-small injection current, which is affected at higher temperature due to the fact that significant portion of the injected carriers populate in the higher energy states before threshold modal gain is reached.

2.3.4 Stability Characterization of Laser Diodes

Figure 2.8 shows the comparison of the aging results under an automatic current control (ACC) condition in the LED mode for the AlGaAs-GaAs laser diodes consisting of the GaAs self-formed islands and the conventional QW structure. The lifetime at 300 K was examined by measuring the output power at a constant injected current density of 500 A/cm^2, which is below the threshold current density. The output power from the quantum well structure decreased rapidly to half of the initial value in 4 minutes. On the other hand, the GaAs island active region reached the half of the initial value after 70 hours. It is believed that the formation of dark line defects in the active region of the QW causes the rapid degradation, whereas, for the laser with island structure in the

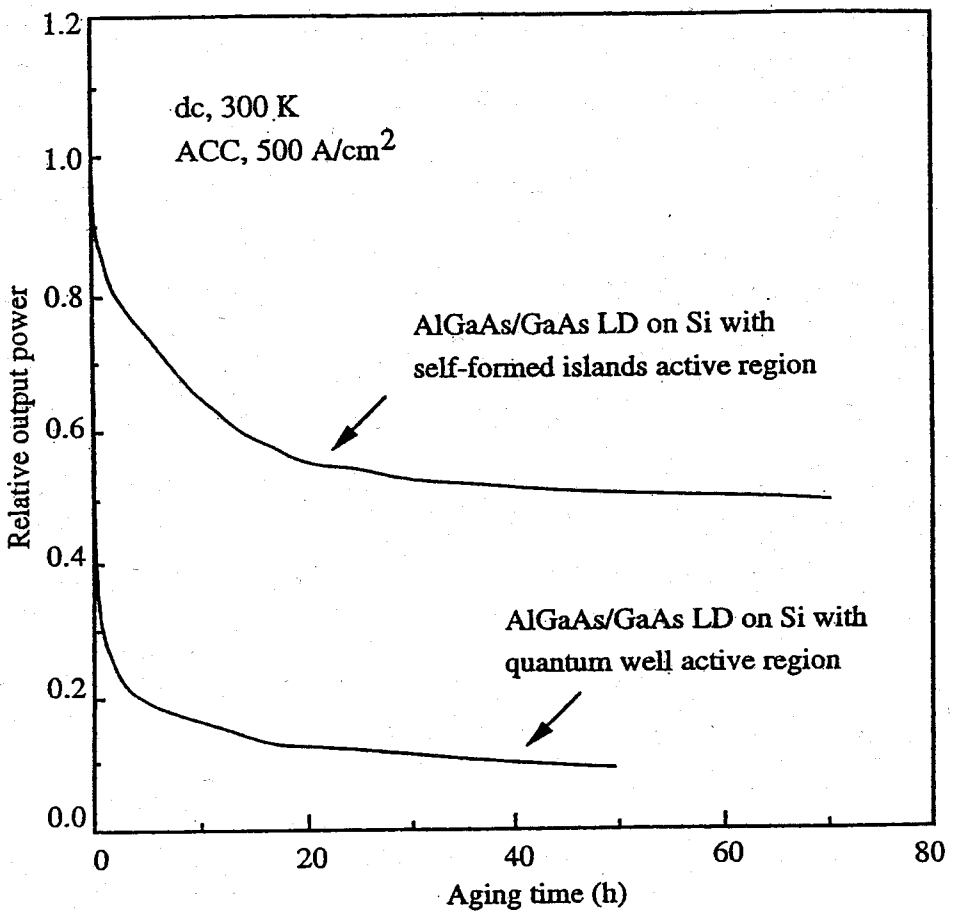

Figure 2.8 : Comparison of aging results for the AlGaAs-GaAs laser diodes on Si with the self-formed GaAs islands and the conventional quantum wells.

active region, the growth of DLD is relieved and hence improves the reliability of the device.

2.4 Conclusions

Laser diodes composed with AlGaAs-GaAs epitaxial layers on Si substrates were grown by MOCVD. Laser diodes with conventional GaAs QW and GaAs self formed islands by droplet epitaxy were realized in order to study the suitability of heteroepitaxial growth of GaAs on Si. Self-formed GaAs islands active regions on Si showed the J_{th} of 5.4 kA/cm^2 under pulsed condition at 300 K, and J_{th} of 3.9 kA/cm^2 under CW condition at 100 K. Lasing was observed at wavelengths of 771 nm and 776 nm under pulsed and CW conditions respectively. The reason for the higher threshold current of the island laser on Si was explained as being due to the lower confining factor of the island structured active region. The operating characteristics such as internal quantum efficiency, internal loss, gain coefficient and transparency current density have been also studied. Further, the island laser on Si shows higher characteristic temperature as well as higher quantum efficiency than those of QW laser on Si. On the basis of aging test investigation, it can be concluded that the self-formed laser diode structure on Si is more reliable than the conventional QW laser diode on Si.

References

1. D. A. B. Miller, D. S. Chemla and S. Schmitt-Rink, Appl. Phys. Lett., **52**, 2154 (1988).
2. Y. Arakawa and A. Yariv, IEEE J. Quantum Electron., **22**, 1887 (1986).
3. L. Banyai, I. Galbraith, C. Ell and H. Haung, Phys. Rev., B **36**, 6099 (1987).
4. F. A. P. Osorio, M. H. Degani and O. Hipolito, Phys. Rev., B **37**, 1402 (1987).
5. H. Sakaki, Jpn. J. Appl. Phys., **19**, L735 (1980).
6. E. Kapon, Proc. IEEEE, **80**, 398 (1992).
7. Y. Arakawa and H. Sakaki, Appl. Phys. Lett., **40**, 939 (1982).
8. M. Asada, Y. Miyamoto and Y. Suematsu, IEEE J. Quantum Electron., **22**, 1925 (1986).
9. H. Sakaki, Jpn. J. Appl. Phys., **28**, L314 (1989).
10. K. J. Vahala, IEEE J. Quantum Electron., **24**, 523 (1988).
11. K. Kash, A. Scherer, J. M. Worlock, H. G. Craighead and M. C. Tamargo, Appl. Phys. Lett., **49**, 1043 (1986).
12. T. Fukui, S. Ando and Y. Tokura, Appl. Phys. Lett., **58**, 2018 (1991).
13. I. N. Stransky and V. L. Krastanov, Akad. Wiss. Lit. Maniz. Natur. Kl. 11b, **146**, 797 (1939).
14. N. Koguchi, S. Takahashi and T. Chikyo, J. Cryst. Growth, **111**, 688 (1991).
15. T. Chikyo, and N. Koguchi, App Phys. Lett., **61**, 2431 (1992).
16. Y. Hasegawa, T. Egawa, T. Jimbo and M. Umeno, *Extended Abstracts of the 1995 Int. Conf. Solid State Devices and Materials*, p. 722 (Osaka, 1995).
17. T. Egawa, A. Ogawa, T. Jimbo and M. Umeno, Jpn. J. Appl. Phys., **37**, 1552 (1998).

18. T. Egawa, Y. Hasegawa, T. Jimbo, and M. Umeno, Jpn. J. Appl. Phys. **31**, 791 (1992).

19. Z. I. Kazi, T. Egawa, T. imbo, and M. Umeno, Jpn. J. Appl. Phys. **38**, 74 (1999).

20. H. Kressel, and J. K. Butler, *Semiconductor Lasers and Heterojunction LEDs*, New York: Academic, p.101 (1977).

21. W. T. Tsang, IEEE J. Quantum Electron., **20**, 1119 (1984).

22. W. Streifer, D. R. Sciferes, and R. D. Burnham, Appl. Opt., **18**, 3547 (1979).

23. D. Botez, RCA Rev. **39**, 577 (1978).

24. L. V. Asryan, and R. A. Suris, IEEE J. Quantum Electron., **34**, 841 (1998).

25. J. P. van der Ziel, R. D. Dupuis, R. A. Logan, R. M. Mikulyak, J. Pizone and A. Savage, Appl. Phys. Lett., **50**, 454 (1987).

26. H. Kressel, and M. Ettenberg, J. Appl. Phys., **47**, 3533 (1976).

27. I. Hayashi, M. B. Panish, and F. K. Reinhart, J. Appl. Phys., **42**, 1929 (1971).

28. M. Ettenberg, C. J. Nuese, and H. Kressel, J. Appl. Phys., **50**, 2949 (1979).

29. J. I. Pankove, IEEE J. Quantum Electron., **4**, 119 (1968).

30. R. K. Ahrenkie, M. M. Al-Jassim, B. Keyes, D. Dunlavy, K. M. Jones, S. M. Vernon, and T. M. Dixon, J. Electrochem. Soc., **137**, 996 (1990).